Journal of Nano Research
ISSN: 1661-9897, Vol. 39, pp 34-42
doi:10.4028/www.scientific.net/JNanoR.39.34
© 2016 Trans Tech Publications, Switzerland
Submitted: 2015-07-16
Revised: 2015-10-30
Accepted: 2015-12-07
Online: 2016-02-18

Enhancement of Electron Spin Relaxation Time in Thin SOI Films by Spin Injection Orientation and Uniaxial Stress

Joydeep Ghosh[1, a *], Dmitry Osintsev[1,b], Viktor Sverdlov[1,c], and Siegfried Selberherr[1,d]

[1]Institute for Microelectronics, TU Wien, Austria

{[a]ghosh, [b]osintsev, [c]severdlov, [d]selberherr}@iue.tuwien.ac.at

Keywords: SOI thin film, Shear strain, Spin-orbit interaction, Spin relaxation, Spin injection orientation

Abstract. The electron spin properties of semiconductors are of immense interest for their potential in spin-driven applications. Silicon is a perfect material for spintronics due to a long spin lifetime. Understanding the peculiarities of the subband structure and details of spin propagation in thin silicon films in the presence of the spin-orbit interaction is under scrutiny. We have performed simulations to obtain the surface roughness limited, acoustic- and optical-phonon mediated spin relaxation time, when the film is under shear strain. The degeneracy between the non-equivalent valleys is lifted by strain, which in turn subdues the dominating inter-valley relaxation components and increases the spin lifetime. We also elaborate on the injection orientation sensitive spin relaxation model and predict that the spin relaxation time is maximum, when the spin is injected in-plane, relative to the (001) oriented silicon film.

Introduction

Growing technological challenges and soaring costs are gradually guiding MOSFET scaling to an end, which drives the search for alternative technologies and computational principles; as predicted by the International Technology Roadmap for Semiconductors (ITRS) [1]. The introduction of a new type of multi-gate three-dimensional transistors has been crucial in the semiconductor industry [2] for continuing the scaling beyond the 22nm down to the 14nm technology node. An obvious saturation of MOSFET miniaturization puts clear foreseeable limitations to the continuation of the increase in the performance of integrated circuits. This is the reason for which intensive research is carried out for alternatives. There have been several investigation areas in 'beyond CMOS', and electron spin-driven applications is one of them.

The fundamental operation of a MOSFET device is based on the charge degree of freedom of the electrons, as the gate induced electric potential manipulates the flow of charge in the channel. On the other hand, electron spin is an additional degree of freedom which could be utilized to build superior devices like a SpinFET which has been proposed a long time ago [3]. In such a device the current modulation can be achieved by tuning the strength of the spin-orbit interaction using the gate voltage. Efficient spin injection with detection, spin transport, and spin manipulation by purely electrical means are immediately required. Although the initial attention was on III-V semiconductors to be used as the channel material because of their high spin-orbit interaction which is necessary for good spin manipulation in a SpinFET structure, silicon is considered to be an important material for spin-driven applications for its long spin lifetime. The estimate for the spin lifetime at room temperature in un-doped silicon is in the order of 10ns. A long transfer distance of conduction electron spins has been shown experimentally [4], hence spin propagation at such distances combined with a possibility of injecting spin at room [5] or even at elevated [6] temperature makes the fabrication of spin-based switching devices quite plausible in the near future. However, a large experimentally observed spin relaxation in electrically-gated silicon structures could become an obstacle in realizing spin-driven devices [7] and hence a deeper understanding of the silicon subband structures and the spin relaxation mechanisms in a confined conducting channel is paramount.

In bulk silicon the conduction electrons are positioned in the vicinity of the minima of the three pairs of equivalent valleys near the edges of the Brillouin zone along the X-, Y-, and Z-axes. Spin scattering in bulk silicon has been studied [8] and it was established that the f-phonons mediated spin-flip processes due to optical phonons (*Op*-phonon) between non-equivalent valleys are responsible for spin relaxation. It has been elaborated that for a thin silicon film of below the nm range, the surface roughness (*SR*), transversal (*TA*)-, and longitudinal (*LA*)-phonon mediated spin relaxation are more dominating than *Op*-phonons in determining spin lifetime [9]. In (001) thin silicon films the confinement leads to the formation of an unprimed subband ladder from the *Z*-valleys and a prime ladder from the *X*(*Y*)-valleys. Due to the difference in the quantization energies the f-processes between the unprimed and primed subbands are suppressed even in unstrained films [10]. Thus, spin relaxation due to the intra- and intersubband transitions between the states with opposite spin projections within the unprimed ladder must be considered.

In this paper a perturbative **k·p** approach is used to describe the electron subband wave functions and energies. The shear strain in [110] direction (ε_{xy}) and the spin-orbit interaction are included [9], [11]. The Hamiltonian is written at the vicinity of the *X*-point along the *Z*-axis in the Brillouin zone. In unstrained films the unprimed subbands are degenerate due to the equivalent valleys degeneracy. The presence of the small but finite spin-orbit term is responsible for a large mixing of the up(down)-spin states between the two unprimed degenerate subbands, resulting in the formation of spin hot spots characterized by strong spin relaxation [9]. In the next part we discuss the relevant Hamiltonian matrix and obtain the subband dispersion and the wave functions. Then the procedure to calculate spin lifetime for different mechanisms is discussed. Finally we investigate the injection direction sensitive spin lifetime in thin silicon films.

TABLE I. Parameter List

Parameters	Value	Unit
Spin-orbit term, Δ_{SO}	1.27	meVnm
Electron rest mass, m_e	$9.1093\cdot10^{-31}$	Kg
Transversal effective mass, m_t	$0.19\cdot m_e$	Kg
Longitudinal effective mass, m_l	$0.91\cdot m_e$	Kg
Shear deformation potential, D	14	eV
Silicon lattice constant, a	$5.431\cdot10^{-10}$	m
Position of the valley minimum relative to the *X*-point in unstrained silicon, k_0	$0.15\cdot2\pi/a$	m^{-1}
Valley splitting at Γ-point (unstrained condition), Δ_Γ	5.5	eV
$k_{0\Gamma}$	$0.85\cdot(2\pi/a)$	m^{-1}
M	$(m_t^{-1}-m_e^{-1})^{-1}$	Kg

Model

Hamiltonian and wave functions:

The effective 4x4 Hamiltonian for the two relevant equivalent valleys along *Z* direction including spin reads

$$H = \begin{bmatrix} H_1 & H_3 \\ H_3 & H_2 \end{bmatrix}, \tag{1}$$

where the components are written as

$$H_{\mathrm{j}=1,2} = [\frac{\hbar^2 k_z^2}{2m_l} + \frac{\hbar^2 (k_x^2+k_y^2)}{2m_t} + (-1)^j \delta + U(z)]\, I \quad (2)$$

$$H_3 = \left[\frac{\hbar^2 k_0 k_z}{m_l}\right] I \quad (3)$$

with $\delta = \sqrt{(D\varepsilon_{xy} - \frac{\hbar^2 k_x k_y}{M})^2 + (k_x^2 + k_y^2)\Delta_{SO}^2 + \lambda_\Gamma^2}.$

Here (k_x, k_y, k_z) denotes the projections of the wave vector, *U(z)* is the confinement potential, and the other parameters are shown in TABLE I. λ_Γ represents the unprimed subband splitting of unstrained silicon (001) films. This valley splitting in the film is incorporated along with ε_{xy} induced valley splitting on equal footing. One can write [13]

$$\lambda_\Gamma = \frac{\Delta_\Gamma \cdot \mathrm{k}_0^3}{{k_0}_\Gamma{}^3}. \quad (4)$$

The eigenfunctions of the Schrödinger equation with the Hamiltonian H for the two lowest unprimed subbands (n=1, 1') with the up(down)-spin states with the spin quantization axis along the spin-orbit field in (k_x, -k_y) direction can be expressed as $\Psi_{n\uparrow}$, $\Psi_{n\downarrow}$. One can use the polar angle θ to denote the spin injection orientation and perform linear transformations to obtain the wave functions $\chi_{n\uparrow}$, $\chi_{n\downarrow}$ with their spins parallel to the injection orientation.

$$\chi_{n\uparrow} = \frac{1}{\sqrt{2}}\left(\cos\left(\frac{\theta}{2}\right) + \sin\left(\frac{\theta}{2}\right).\mathrm{e}^{-\mathrm{i}\varnothing_1}\right)\Psi_{n\uparrow} + \frac{1}{\sqrt{2}}\left(\cos\left(\frac{\theta}{2}\right) - \sin\left(\frac{\theta}{2}\right).\mathrm{e}^{-\mathrm{i}\varnothing_1}\right)\Psi_{n\downarrow} \quad (5)$$

$$\chi_{n\downarrow} = \frac{1}{\sqrt{2}}\left(-\sin\left(\frac{\theta}{2}\right) + \cos\left(\frac{\theta}{2}\right).\mathrm{e}^{-\mathrm{i}\varnothing_1}\right)\Psi_{n\uparrow} + \frac{1}{\sqrt{2}}\left(-\sin\left(\frac{\theta}{2}\right) - \cos\left(\frac{\theta}{2}\right).\mathrm{e}^{-\mathrm{i}\varnothing_1}\right)\Psi_{n\downarrow} \quad (6)$$

$$\tan \varnothing_1 = -\frac{k_y}{k_x}.$$

The Hamiltonian (1) for the primed subbands with Z quantization axis can be represented as [13]

$$H' = \begin{bmatrix} H_1' & H_3' \\ H_3' & H_2' \end{bmatrix}, \quad (7)$$

where the components are

$$H'_{\mathrm{j}=1,2} = [\frac{\hbar^2 k_z^2}{2m_l} + \frac{\hbar^2 (k_x^2+k_y^2)}{2m_t} (-1)^j \frac{\hbar^2 k_x k_y}{\mathrm{M}} + \mathrm{U(z)}]\, I, \quad (8)$$

$$H'_3 = \left[\frac{\hbar^2 k_0 k_z}{m_l}\right] I. \quad (9)$$

Spin lifetime calculations:

The general framework for the spin lifetime (τ) calculations is outlined below. The spin relaxation rate can be expressed by

$$\frac{1}{\tau} = \frac{\int \frac{1}{\tau(\boldsymbol{K_1})} f(E)(1-f(E))\, d\boldsymbol{K_1}}{\int f(E)\, d\boldsymbol{K_1}}, \quad (10)$$

where $f(E) = \frac{1}{1+\exp(\frac{E-E_F}{K_B T})}$, $\int d\boldsymbol{K_1} = \int_0^{2\pi} d\emptyset \int_0^{\infty} \frac{|\boldsymbol{K_1}(\emptyset,E)|}{|\frac{\partial E(\boldsymbol{K_1})}{\partial \boldsymbol{K_1}}|} dE$.

E is the electron energy, $\boldsymbol{K_1}$ is the in-plane wave vector, K_B is the Boltzmann constant, T is the temperature, and E_F is the Fermi level.

(A). Surface roughness:

The *SR*-induced spin (momentum) relaxation rate is calculated as

$$\frac{1}{\tau_{\mathrm{SR}}(\mathbf{K_1})} = \frac{4(2)\pi}{\hbar(2\pi)^2} \sum_{i,j} \int_0^{2\pi} \pi \Delta^2 L^2 \frac{1}{\epsilon_{ij}^2(\boldsymbol{K_2}-\boldsymbol{K_1})} \frac{\hbar^4}{4m_l^2} \frac{|\boldsymbol{K_2}|}{|\frac{\partial E(\boldsymbol{K_2})}{\partial \boldsymbol{k_2}}|} [(\frac{d\chi_{i\boldsymbol{K_1}\sigma}}{dz})^* (\frac{d\chi_{j\boldsymbol{K_2}-\sigma(\sigma)}}{dz})]^2_{z=\pm\frac{t}{2}} \cdot \exp\left(\frac{-(\boldsymbol{K_2}-\boldsymbol{K_1})^2 L^2}{4}\right) d\emptyset \quad (11)$$

$\boldsymbol{K_1}$, $\boldsymbol{K_2}$ are the in-plane wave vectors before and after scattering, $\emptyset$ is the angle between $\boldsymbol{K_1}$ and $\boldsymbol{K_2}$, ϵ is the dielectric permittivity, L is the autocorrelation length, Δ is the mean square value of the surface roughness fluctuations, and $\sigma=\pm1$ is the spin projection to the [001] axis.

(B). Phonons:

The electron-phonon scattering induced momentum relaxation rates are evaluated in a standard way [14]. The intravalley spin relaxation due to *TA*-phonons is computed as

$$\frac{1}{\tau_{\mathrm{TA}}(\mathbf{K_1})} = \frac{\pi K_B T}{\hbar \rho \vartheta_{TA}^2} \sum \int_0^{2\pi} d\emptyset \frac{|\boldsymbol{K_2}|}{|\frac{\partial E(\boldsymbol{K_2})}{\partial \boldsymbol{k_2}}|} \left[1 - \frac{\frac{\partial E(\boldsymbol{K_2})}{\partial \boldsymbol{K_2}} f(E(\boldsymbol{K_2}))}{\frac{\partial E(\boldsymbol{K_1})}{\partial \boldsymbol{K_1}} f(E(\boldsymbol{K_1}))}\right] \cdot \int_0^t \int_0^t \exp(-\sqrt{q_x^2+q_y^2}|z-z'|) [\chi_{\boldsymbol{K_2}\sigma}^{\dagger}(z) M \chi_{\boldsymbol{K_1}_{-\sigma}}(z)]^* [\chi_{\boldsymbol{K_2}\sigma}^{\dagger}(z') M \chi_{\boldsymbol{K_1}_{-\sigma}}(z')] \cdot \left[\sqrt{q_x^2+q_y^2} - \frac{8q_x^2 q_y^2 - (q_x^2+q_y^2)^2}{q_x^2+q_y^2} |z-z'|\right] dz dz' \quad (12)$$

where ρ=2329kg/m^3 is the silicon density, υ_{TA}=5300m/s is the transversal phonons velocity, t is the film thickness, $(q_x, q_y)=\boldsymbol{K_1}-\boldsymbol{K_2}$, and M written in the two valley plus two spin projection basis as:

$$M = \begin{bmatrix} 0 & 0 & \frac{D}{2} & 0 \\ 0 & 0 & 0 & \frac{D}{2} \\ \frac{D}{2} & 0 & 0 & 0 \\ 0 & \frac{D}{2} & 0 & 0 \end{bmatrix}.$$

The intravalley spin relaxation rate due to the *LA*-phonons is calculated as

$$\frac{1}{\tau_{\mathrm{LA}}(\mathbf{K_1})} = \frac{\pi K_B T}{\hbar \rho \vartheta_{LA}^2} \sum \int_0^{2\pi} d\emptyset \frac{|\boldsymbol{K_2}|}{\frac{\partial E(\boldsymbol{K_2})}{\partial \boldsymbol{k_2}}} \left[1 - \frac{\frac{\partial E(\boldsymbol{K_2})}{\partial \boldsymbol{K_2}} f(E(\boldsymbol{K_2}))}{\frac{\partial E(\boldsymbol{K_1})}{\partial \boldsymbol{K_1}} f(E(\boldsymbol{K_1}))}\right] \cdot \int_0^t \int_0^t \exp(-\sqrt{q_x^2+q_y^2}|z-z'|) \cdot [\chi_{\boldsymbol{K_2}\sigma}^{\dagger}(z) M \chi_{\boldsymbol{K_1}_{-\sigma}}(z)]^* [\chi_{\boldsymbol{K_2}\sigma}^{\dagger}(z') M \chi_{\boldsymbol{K_1}_{-\sigma}}(z')] \cdot \frac{4q_x^2 q_y^2}{(q_x^2+q_y^2)^{\frac{3}{2}}} [\sqrt{q_x^2+q_y^2}|z-z'| + 1] dz dz' \quad (13)$$

where υ_{LA}=8700m/s is the speed of the longitudinal phonons.

The intervalley spin relaxation rate due to acoustic phonons contains the Elliot and Yafet mechanism [8], and can be written as

$$\frac{1}{\tau_{\mathrm{LA}}(\mathbf{K_1})} = \frac{\pi K_B T}{\hbar\rho\vartheta_{LA}^2}\sum\int_0^{2\pi} d\emptyset \frac{|\boldsymbol{K_2}|}{|\frac{\partial E(\boldsymbol{K_2})}{\partial k_2}|}\left[1-\frac{\frac{\partial E(\boldsymbol{K_2})}{\partial \boldsymbol{K_2}} f(E(\boldsymbol{K_2}))}{\frac{\partial E(\boldsymbol{K_1})}{\partial \boldsymbol{K_1}} f(E(\boldsymbol{K_1}))}\right].\int_0^t [\chi_{\boldsymbol{K_2}\sigma}^{\dagger}(z) M' \chi_{\boldsymbol{K_{1-\sigma}}}(z)]^* . [\chi_{\boldsymbol{K_2}\sigma}^{\dagger}(z) M' \chi_{\boldsymbol{K_{1-\sigma}}}(z)] dz \quad (14)$$

where the matrix M' is

$$M' = \begin{bmatrix} D' & 0 & 0 & D_{SO}(q_y - iq_x) \\ 0 & D' & D_{SO}(-q_y - iq_x) & 0 \\ 0 & D_{SO}(-q_y + iq_x) & D' & 0 \\ D_{SO}(q_y + iq_x) & 0 & 0 & D' \end{bmatrix}$$

with D'=12eV, D_{SO}=15meV/k_0 [8].

The intervalley spin relaxation rate due to the *Op*-phonons between unprimed and primed subbands is calculated as

$$\frac{1}{\tau_{\mathrm{OP}}(\mathbf{K_1})} = \frac{2\pi}{\rho\omega_{op}}\sum\rho_2(E_1 \mp \hbar\omega_{op})\left[\frac{1-f(E(\boldsymbol{K_1})\mp\hbar\omega_{op})}{1-f(E(\boldsymbol{K_2}))}\right].\left(n_{op}+\frac{1}{2}\pm\frac{1}{2}\right).\int_0^t [|\chi_{\boldsymbol{K_2}}^{\dagger}(z) M^{OP} \chi_{\boldsymbol{K_1}}(z)|]^2 dz\,, \quad (15)$$

where $n_{op} = \frac{1}{e^{(\frac{\hbar\omega_{op}}{K_B T})}-1}$ is the Bose occupation factor, ω_{op} denotes the frequency of the optical phonons, $\rho_j(E)$ is the density of states for subband j (=1,2), and M^{OP} is expressed as

$$M^{OP} = \begin{bmatrix} 0 & D_{op} & 0 & D_{op} \\ D_{op} & 0 & D_{op} & 0 \\ 0 & D_{op} & 0 & D_{op} \\ D_{op} & 0 & D_{op} & 0 \end{bmatrix},$$

with D_{op}=6.5meV·(2π/a) [8].

Results

Figure 1 shows the spin injection orientation with respect to the quantization axis of a (001) thin silicon film, defined by θ. The subband wave functions have 4 components, including two valleys with two spin projections. For perpendicular-plane spin injection the up(down)-spin wave function consists of large and small components, where the small component pertains to the down(up)-spin component within it. Their absolute value depends on the $\boldsymbol{k}$ vector and ε_{xy}. The applied shear strain reduces the small component [12], thus reducing the spin mixing between up- and down spin states in different valleys, and therefore the spin scattering (lifetime) is decreased (increased). We notice that, for any arbitrary ε_{xy} and in-plane wave vector (k_x, k_y), the absolute value of the large (small) component is reduced (increased), when the spin injection direction is changed from perpendicular(*OZ*-direction)- to in(*OX*-direction)-plane, as shown in Figure 2. However under similar conditions, the intersubband *SR*-induced spin relaxation matrix elements normalized to intrasubband scattering (M_{SR}) is reduced for an in-plane spin injection (Figure 3). M_{SR} attains its maximum, when the spin hot spot condition ($D\varepsilon_{xy} - \frac{k_x k_y}{M}$) $= 0$ is met [15], and then gradually decreases with increasing ε_{xy}. The energy splitting between the lowest unprimed subbands (valley splitting) also shown in Figure 3, remains insensitive to θ as expected. The valley splitting reaches its minimum at the spin hot spot condition. With ε_{xy} increased, the hot spots are pushed to higher energies towards the unoccupied states, which results in a spin lifetime enhancement.

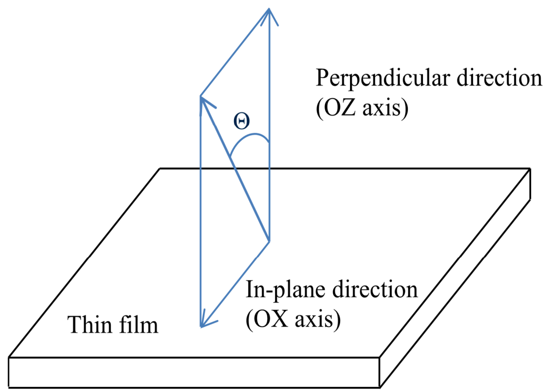

Figure 1. Thin (001) oriented film of thickness t, with the spin injection orientation described by the polar angle θ.

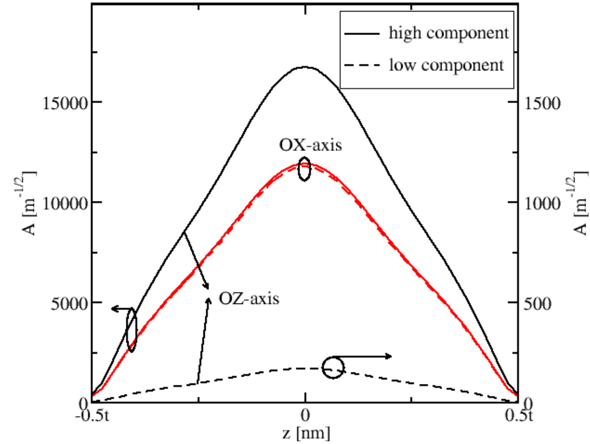

Figure 2. The absolute value of the high (small) component of the spin wave function is reduced (increased), when the spin injection orientation is drawn from the OZ-axis to the OX-axis. k_x=0.4nm, k_y=0.4nm, ε_{xy}=0.5%, and t=4.34nm.

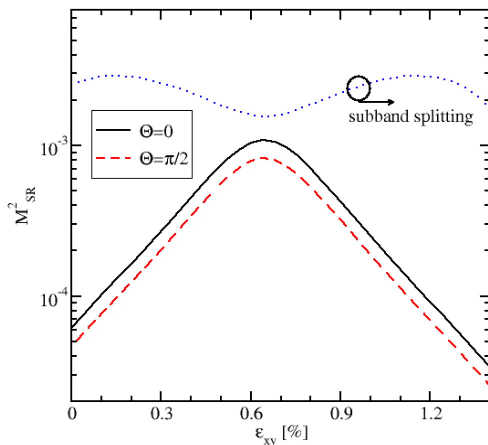

Figure 3. The intersubband SR-induced spin relaxation matrix element normalized to intrasubband scattering is reduced, when the spin injection orientation is drawn towards the OX-axis. t=4.34nm, k_x=0.4nm^{-1}, k_y=0.7nm^{-1}.

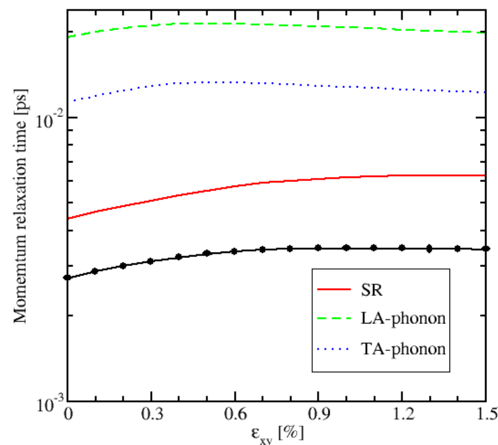

Figure 4. The momentum relaxation time and its different components with ε_{xy}. T=443K, t=1.36nm, and the electron concentration (N_S)= $1.29\cdot10^{12}$cm^{-2}.

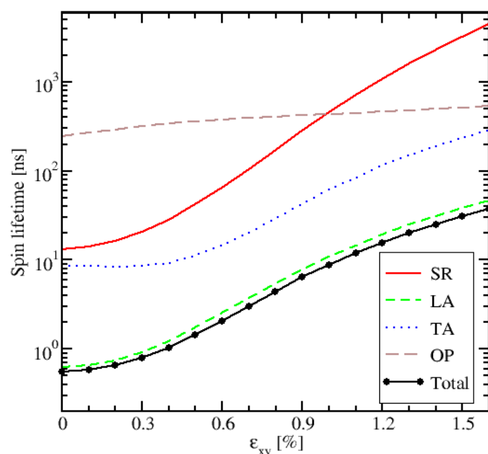

Figure 5. The variation of the spin lifetime and its components with ε_{xy}. T=300K, t=4.34nm, N_S=$1.29\cdot10^{12}$ cm^{-2}.

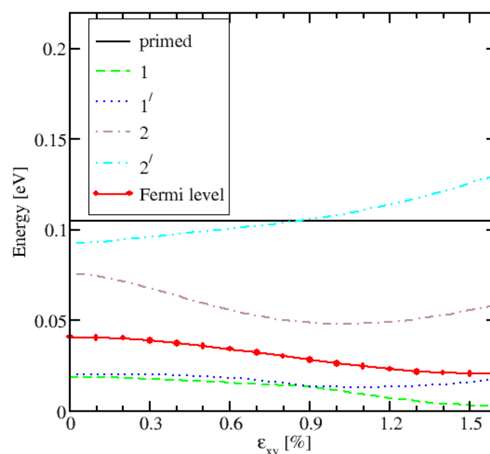

Figure 6. Energies of the lowest (1) and second lowest (2) unprimed subbands, with the primed band energy and the Fermi level. t=4.34nm, T=300K.

We proceed further to compute the momentum relaxation time (τ^M) for all different mechanisms, depicted in Figure 4. It is observed that θ does not have any influence on τ^M as envisioned. In thin films *SR*-mediated momentum scattering is found to be the dominating mechanism as observed from Figure 4. It is also spotted that the momentum relaxation time can be increased by a factor of two at the most with ε_{xy}.

Figure 5 shows the spin lifetime (τ) with its components due to all distinct mechanisms, showing a large increment with ε_{xy}, for all cases. This is mediated by the ε_{xy} induced splitting between the [001] valley pair. Along with the effect of *SR* and acoustic-phonon induced scattering, both of which are increased by orders of magnitude with ε_{xy}, we have also included the effect of *Op*-phonons. The latter is primarily responsible for spin relaxation in bulk silicon [11]. We notice that for a t=4.34nm film, *LA*-phonons have a major contribution in determining τ, whereas the *SR* mechanism hardly influences τ. The increase of the spin lifetime mediated by *Op*-phonons with ε_{xy} is not severe. For thicker films (film thickness larger than 7nm), the effect of a several orders of magnitude increase of τ in strained films should be mitigated.

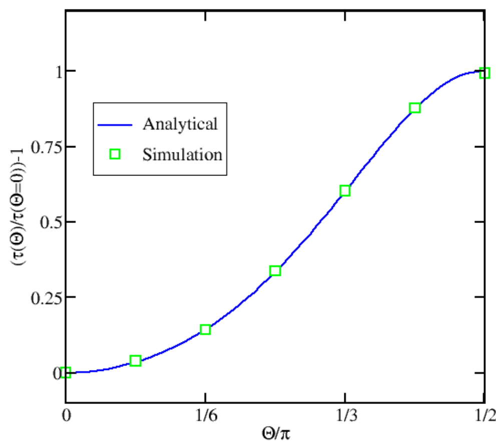

Figure 7. Variation of τ with θ. t=4.34nm. ε_{xy}=0.5%.

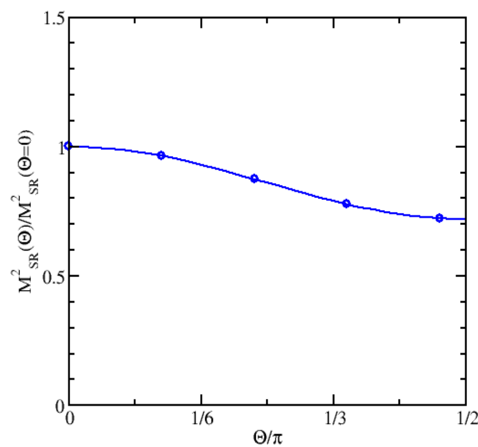

Figure 8. Variation of M_{SR} with θ. t=4.34nm, k_x=0.4nm^{-1}, k_y=0.7nm^{-1}. Dots: simulation.

The dependence of the energies for unprimed subbands on ε_{xy} for k_x=0, k_y=0 together with the Fermi energy is shown in Figure 6. Energy 1 and Energy 1' stand for the lowest subbands representing the symmetric and asymmetric wave function combination of the two opposite valleys along [001] direction. Energy 2 and Energy 2' stand for the next unprimed subbands. ε_{xy} lifts the degeneracy between Energy 1 (2) and Energy 1' (2'). This lifting of the degeneracy is the crucial factor for spin lifetime enhancement. We note that the degeneracy between the equivalent valleys was a longstanding problem in silicon spintronics. The minimum energy of the primed subband is located at the point k_z=k_0, k_y=0, and its position is also shown in Figure 6. Because of the difference in the energies between the lowest primed and unprimed subbands, *Op*-phonons are less important in determining the value of τ in thin films. Nevertheless, the importance increases when the thickness is further increased.

Next we investigate, how one can express the variation of τ on θ, at any fixed ε_{xy} point. In Figure 7 we highlight the ratio of τ for any arbitrary value of θ compared to that for perpendicular-plane injection at ε_{xy}=0.5%. An analytical expression describing this dependence is observed to be

$$\tau(\theta) \propto \frac{1}{1+(\cos\theta)^2} \tag{16}$$

`

and thus $\tau\left(\theta = \frac{\pi}{2}\right) = 2 \cdot \tau(\theta = 0)$. The simulated results and the analytical expression show perfect agreement. The injection orientation dependence can be correlated to the variation of M_{SR}

with θ, which can be expressed (Figure 8) as: $M_{SR}(\theta) \propto \frac{1}{1+(\frac{k_x}{k_y})^2\cdot(\cos\theta)^2}$ (valid for any arbitrary pair of k_x, k_y). We point out that a similar dependence of the spin lifetime on the injection orientation with respect to the valley orientation axis has also been reported for bulk silicon [16], [17], indicating that the result (16) is more general as it is applicable in both bulk silicon and thin silicon films.

Summary

An effective **k·p** Hamiltonian with spin degree of freedom is used to find the subband wave functions and the subband energies in the presence of strain and spin-orbit interaction in thin silicon films. We have discussed, how shear strain-induced subband splitting causes a giant increment of the spin lifetime in such a film, whereas only a two-fold increase of the momentum relaxation time is noticed. We observe that for a film thickness larger than 2.5nm acoustic phonons are instrumental in determining the spin lifetime, while surface roughness is dominant for thinner films. We have also shown that an alteration of the spin injection direction further influences the individual spin relaxation rates and henceforth the total spin lifetime, but does not affect the momentum relaxation time. When the spin injection orientation is drawn towards in-plane, it is observed that the intersubband spin relaxation matrix elements get reduced with shear strain, and accordingly the spin relaxation rate for all distinct mechanisms decreases and hence the spin lifetime increases. We predict a two-fold increase of the spin lifetime, when spins are injected in-plane, compared to when they are injected perpendicular-plane.

This work is supported by the European Research Council through the grant #247056 MOSILSPIN.

References

[1] International technology roadmap for semiconductors (ITRS), http://www.itrs.net (2013).

[2] M. Bohr, The evolution of scaling from the homogeneous era to the heterogeneous era, IEDM, pp. 1.1.1-1.1.6 (2011).

[3] S. Datta and B. Das, Electronic analog of the electro-optic modulator, Appl. Phys. Lett. 56(7), 665 (1990).

[4] B. Huang, D.J. Monsma, and I. Appelbaum, Coherent spin transport through a 350 micron thick silicon wafer, Phys. Rev. Lett. 99, 177209 (2007).

[5] S.P. Dash, S. Sharma, R.S. Patel, M.P. de Jong, and R. Jansen, Electrical creation of spin polarization in silicon at room temperature, Nature 462, 491 (2009).

[6] C.H. Li, O.M.J. van 't Erve, and B.T. Jonker, Electrical injection and detection of spin accumulation in silicon at 500K with magnetic metal/silicon dioxide contacts, Nature Commun. 2, 245 (2011).

[7] J. Li and I. Appelbaum, Modeling spin transport in electrostatically-gated lateral-channel silicon devices: Role of interfacial spin relaxation, Phys. Rev. B 84, 165318 (2011).

[8] Y. Song and H. Dery, Analysis of phonon-induced spin relaxation processes in silicon, Phys. Rev. B 86, 085201 (2012).

[9] D. Osintsev, V. Sverdlov, and S. Selberherr, Electron mobility and spin lifetime enhancement in strained ultra-thin silicon films, Solid-State Electron. 112, 46 (2015).

[10] J.M. Tang, B.T. Collins, and M.E. Flatté, Electron spin-phonon interaction symmetries and tunable spin relaxation in silicon and germanium, Phys. Rev. B 85, 045202 (2012).

[11] P. Li and H. Dery, Spin-orbit symmetries of conduction electrons in silicon, Phys. Rev. Lett. 107, 107203 (2011).

[12] D. Osintsev, V. Sverdlov, N. Neophytou, and S. Selberherr, Valley splitting and spin lifetime enhancement in strained thin silicon films, IWCE Proc. (2014).

[13] V. Sverdlov, Strain-induced effects in advanced MOSFETs, Springer (2011).

[14] M.V. Fischetti, Z. Ren, P.M. Solomon, M. Yang, and K. Rim, Six-band **k·p** calculation of the hole mobility in silicon inversion layers: Dependence on surface orientation, strain, and silicon thickness, J. Appl. Phys. 94, 1079 (2003).

[15] V. Sverdlov and S. Selberherr, Silicon spintronics: Progress and challenges, Physics Reports 585, 1 (2015).

[16] H. Dery, Y. Song, P. Li, and I. Zutic, Silicon spin communication, Appl. Phys. Lett. 99, 082502 (2011).

[17] J. L. Cheng, M. W. Wu, and J. Fabian, Theory of the spin relaxation of conduction electrons in silicon, Phys. Rev. Lett. 104, 016601 (2010).